EUROPEAN ORGANIZATION FOR NUCLEAR RESEARCH

AB-Note-2008-001 ABP
CARE-Note-2007-012-HHH

Loss of Longitudinal Landau Damping in the LHC Injectors

Ibon Santiago González
University of the Basque Country, Bilbao

Abstract

A large number of collective instability mechanisms act on high-intensity beams. It is necessary to determine under what conditions the beam will remain stable. Space charge is the most fundamental mechanism and it represents the main intensity limitation in low-energy machines, while at high energy the inductive chamber impedance is often dominant. Landau damping provides a natural stabilizing mechanism against collective effects, if particles in the beam have a small spread S in their natural frequencies. The purpose of this report is to study the loss of *Landau damping* for the longitudinal plane via the "Sacherer formalism". Stability limits are calculated for several longitudinal beam distributions, including two types of flat bunches, which could be of interest to the LHC upgrade. Landau stability diagrams are computed and presented for different azimuthal modes. A general recipe is given for calculating the threshold intensity in the case of a capacitive impedance below transition or, equivalently, for a purely inductive impedance above transition. Results are finally applied to the case of the PS Booster, as an example of space-charge impedance below transition, and to the SPS, as an example of inductive impedance above transition.

We acknowledge the support of the European Community-Research Infrastructure Activity under the FP6 "Structuring the European Research Area" programme (CARE, contract number RII3-CT-2003-506395).

Geneva, Switzerland

January 5, 2008

1 Introduction

It is known that circulating bunched beams induce electromagnetic fields in the vacuum pipe giving rise to image currents that act back on the beam. Under certain conditions the beam will become unstable. This is a general mechanism that drives an *instability*.

The vacuum chamber, having a finite conductivity, presents an *impedance* to the beam image current. The impedance $Z = Z_r + iZ_i$ can be resistive (real, $Z_i = 0$), capacitive (imaginary, $Z_i > 0$) or inductive ($Z_i < 0$). The voltage induced is given by $V \sim IZ$.

Following Sacherer [1] we can represent the beam particle distribution as the sum of a stationary (time independent) component g_0 and a small perturbtation term g_1 of the form

$$g(r, \theta, t) = g_0(r, \theta) + g_1(r, \theta, t)e^{-\imath\Omega t} \ , \tag{1}$$

where r and θ are polar coordinates in the longitudinal phase space[1], representing the amplitude and phase of the synchrotron motion, respectively, i.e.

$$\phi = r\cos\theta \tag{2}$$

$$\frac{\dot{\phi}}{\omega_{sc0}} = r\sin\theta \ . \tag{3}$$

Here ϕ denotes the phase of a particle with respect to the rf wave (divided by 2π) and ω_{sc0} the angular frequency of the longitudinal motion at the centre of the bunch including the incoherent synchrotron frequency shift (with respect to the synchotron frequency ω_{s0} of a single particle) $\Delta\omega_{incoh}$ due to the potential-well distortion induced by the stationary distribution, i.e.

$$\omega_{sc0} = \omega_{s0} + \Delta\omega_{incoh} \ . \tag{4}$$

The incoherent frequency shift $\Delta\omega_{incoh}$ is negative for a capacitive impedance (e.g. space charge) below transition or for an inductive impedance above transition. The evolution of the perturbed particle distribution g_1 is governed by the Vlasov equation [1, 2].

The longitudinal impedance leads to a complex frequency shift $\Delta\Omega$ that perturbs the original angular frequency of the motion of the mth order longitudinal mode, which becomes $\Omega = m\omega_{sc0} + \Delta\Omega$.

If nonlinearities are neglected, the longitudinal motion of a particle due to an external rf voltage resembles that of the harmonic oscillator and no frequency spread is present. In this case the beam is either stable or unstable for any current and, when unstable, the growth rate of the instability will depend on the bunch population. In the presence of a frequency spread the fact that not all particles in the beam oscillate with the same frequency, *Landau damping* occurs and stabilizes the beam under certain conditions. It is the purpose of this report to study when this natural stabilizing

[1] As Sacherer, we will assume that the synchrotron frequency ω_s is a function of the phase space amplitude r, but that it does not vary very much between the bunch-center and the bunch edge, which makes the problem more tractable because with such a small perturbation, the trajectories of the particles in phase space z, p_z will be nearly circular, and the evolution of various modes can be decoupled. However, this assumption may not always be fulfilled for proton beams which often occupy most of the rf bucket.

mechanism is lost and provide realistic intensity thresholds above which the beam will become unstable.

The perturbation $g_1(r,\theta)$ can be written in the form [1, 2]

$$g(r,\theta,t) = \sum_{m=1}^{\infty} R_m e^{-\imath m\theta} e^{-\imath\Omega t} \tag{5}$$

as the distribution must be periodic in θ with a period 2π, where R_m are radial functions corresponding to the m^{th} azimuthal mode that are defined from the linearized Vlasov equation (applying to small perturbations of the stationary distribution).

If the change in mode frequency due to the impedance is small, so that $\Omega - m\omega_{sc} \ll \omega_{sc}$, the coupling between different azimuthal modes can be neglected, leading to the *Sacherer integral equation* for a single mode m:

$$(\Omega - m\omega_{sc}(r))R_m(r) = \frac{dg_0}{dr}\int_0^{\infty} G_m(r,r')R_m(r')r'dr' \tag{6}$$

where the matrix $G_m(r,r')$ is given by

$$G_m(r,r') = \frac{\imath e^2 v}{2\pi C}\int_0^{2\pi} d\theta \int_0^{2\pi} d\theta' K_m(r'\cos\theta' - r\cos\theta)\sin\theta e^{\imath m(\theta'-\theta)} \tag{7}$$

The *synthetic kernel approach* [3, 4] is normally used to solve Eq. (6). In this approach, the actual interaction that generates an infinity of modes is replaced by a simplified interaction that excites only the rigid-dipole mode for $m = 1$, or, equivalently, only one of any of the other, higher-order, rigid multipole modes [2]. For a general mode of order m, the synthetic kernel is of the form [4]

$$K_m \propto r'^{m-1} r^m \ . \tag{8}$$

Using this dependence in (7) yields $G_m(r,r') = C_m r^m r'^{m-1}$, where all constants have been absorbed into C_m. Finally, with the synthetic kernel Sacherer's equation (6) can be rewritten as

$$1 = C_m \int_0^{\infty} \frac{r^{2m}\frac{dg_0}{dr}dr}{\Omega - m\omega_{sc}(r)} \ . \tag{9}$$

1.1 Definition of $\Delta\omega_m$

In the absence of frequency spread, the denominator in (9) can be taken out of the integral because it is constant, $\Omega - m\omega_{sc}(r) = \Omega - m\omega_{sc0}$. We can thus define $W_m = \int_0^{\infty} r^{2m}\frac{dg_0}{dr}dr$ and $\Delta\omega_m = \Omega - m\omega_{sc}$ as the "dynamic coherent frequency shift". This yields the well-known *Sacherer dispersion relation* (Eq. (16) in Ref. [1]):

$$1 = \frac{\Delta\omega_m}{W_m}\int_0^{\infty} \frac{r^{2m}\frac{dg_0}{dr}dr}{\Omega - m\omega_{sc}(r)} \tag{10}$$

[2] For the lowest mode, i.e. the dipole mode $m = 1$, Ng [4] assumes a force proportional to the longitudinal distance namely $K_1 = A(r'\cos\phi' - r\cos\phi)$. The implications and the correctness of Ng's ansatz should be explored in the future.

1.2 Incoherent and coherent frequency shifts

The coherent synchrotron frequency of the bunch is,

$$\Omega = m\omega_{s0} + m\Delta\omega_{incoh} + \Delta\omega_m \equiv m\omega_{sc0} + \Delta\omega_m \ , \tag{11}$$

where we distinguish an incoherent frequency shift at the bunch center, $\Delta\omega_{incoh}$ and the dynamic coherent shift introduced above.

For an elliptical distribution, i.e. parabolic line density, E. Metral [5], K.Y. Ng [4], and also earlier F. Ruggiero [6], pointed out that in the absence of synchrotron frequency spread, the coherent frequency shift of the rigid dipole mode $m = 1$ vanishes. This feature can be understood from a simple physical argument, namely from the fact that the rigid-dipole motion of the bunch center will not be affected by the wake field because the sum of all internal forces is zero. For this reason the coherent frequency must be just equal to the bare synchrotron frequency. This situation is sketched in Fig. 1.

The synchrotron frequency spread vanishes for small amplitudes (i.e. for bunches occupying a small fraction of the bucket) and with a constant de-focusing (or focussing) self-force. In the case of a purely (positive or negative) inductive impedance, the focusing (or defocusing) self force is constant for a parabolic line density.

However, to study loss of Landau damping the frequency spread arising from the nonlinearity of the external rf wave and the finite length of the bunch is essential and cannot be neglected. In the following discussion stability diagrams for different distributions and azimuthal modes will be analyzed including a nonzero (normalized) frequency spread S.

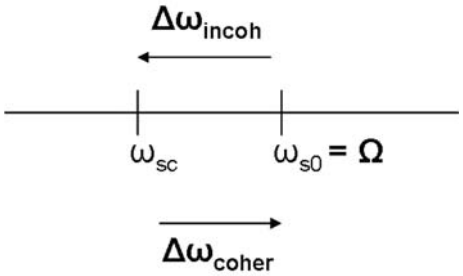

Figure 1: Graphical representation of the case of a capacitive impedance below transition with no frequency spread for the dipole mode

2 Distributions in the longitudinal phase space and its projections using the Abel transformation

The discussion on Landau damping that is derived from the Sacherer dispersion relation in (10) depends on the choice of longitudinal phase space distribution $g(r)$. Its projection onto the z-axis gives the line density $\lambda(z)$ and this is what normally one can measure.

For an approximately circular distribution $g(r)$ in normalized phase space a projection onto the axis can be performed using the Abel transformation, first introduced in [7].

The Abel transform of a function $g(r)$ that is rotationally symmetric is given by

$$\lambda(z) = 2\int_z^{\hat{\tau}} \frac{g(r)rdr}{\sqrt{r^2 - z^2}} \ , \tag{12}$$

where $g(r)$ is taken to be normalized such that in polar coordinates the following applies

$$2\pi \int_0^{\hat{\tau}} g(r)rdr = 1 \ . \tag{13}$$

Throughout this report we will take z to designate the length coordinate (or τ the time, alternatively) and $\hat{\tau}$ to denote the half bunch length.

Let us consider some commonly used distributions. As a first example, the elliptical density distribution

$$g(r) = \frac{3}{2\pi\hat{\tau}^2}\sqrt{1 - \frac{r^2}{\hat{\tau}^2}} \qquad 0 < r < \hat{\tau} \tag{14}$$

has the parabolic linear projection

$$\lambda(z) = \frac{3}{4\hat{\tau}}\left(1 - \frac{z^2}{\hat{\tau}^2}\right) \qquad 0 < |z| < \hat{\tau} \ . \tag{15}$$

Both functions are illustrated in Fig. 2. The projection λ has a discontinuity in its derivative right at the end of the bunch.

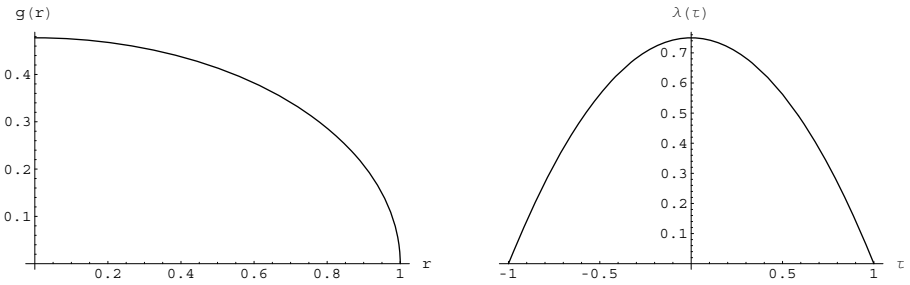

Figure 2: Elliptical distribution $g(r) = 3/(2\pi\hat{\tau}^2)\sqrt{1 - \frac{r^2}{\hat{\tau}^2}}$ of (14) and its projection $\lambda(z)$ of (15), where the half bunch length has been set to one ($\hat{\tau} = 1$) for convenience.

To avoid the problem of discontinuous derivative, a parabolic density distribution may be used of the form

$$g(r) = \frac{2}{\pi\hat{\tau}^2}\left(1 - \frac{r^2}{\hat{\tau}^2}\right) \qquad 0 < r < \hat{\tau} \ , \tag{16}$$

whose corresponding projection is given by its Abel transform as

$$\lambda(z) = \frac{8}{3\pi\hat{\tau}}\left(1 - \frac{z^2}{\hat{\tau}^2}\right)^{3/2} \qquad 0 < |z| < \hat{\tau} \ . \tag{17}$$

In his original paper, F. Sacherer [1] used a smooth distribution with zero slope at the beam edge,

$$g(r) = \frac{3}{\pi\hat{\tau}^2}\left(1 - \frac{r^2}{\hat{\tau}^2}\right)^2 \qquad 0 < r < \hat{\tau}\ . \tag{18}$$

The projection of this function,

$$\lambda(z) = \frac{16}{5\pi\hat{\tau}}\left(1 - \frac{z^2}{\hat{\tau}^2}\right)^{5/2} \qquad 0 < |z| < \hat{\tau}\ , \tag{19}$$

is well-behaved. Both g and λ for the smooth distribution are shown in Fig. 3.

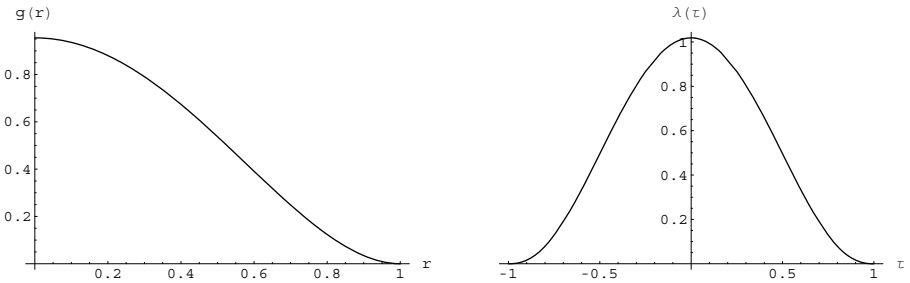

Figure 3: Smooth distribution $g(r) = (3/\pi\hat{\tau}^2)\left(1 - \frac{r^2}{\hat{\tau}^2}\right)^2$ of (18) and its projection $\lambda(z)$ of (19) onto the time axis.

2.1 Parameter dependent parabolic-like distributions

The three previous density functions are all examples of a more general class of distributions that can be expressed in terms of a free parameter n [8]:

$$g(r) = \frac{n+1}{\pi\hat{\tau}^2}\left(1 - \frac{r^2}{\hat{\tau}^2}\right)^n \ 0 < r < \hat{\tau}\ . \tag{20}$$

From this, we recover the elliptic distribution for $n = 1/2$ and the smooth distribution for $n = 2$. In a recent report by K.Y. Ng [4] the stability diagrams for several different example values of n are analyzed. An analytic solution of the dispersion relation for the general parabolic-like distribution of the type (20) exists, which was derived by F. Ruggiero and S. Berg [8]. The Abel transformation of such functions can also be calculated and it can written in the compact form

$$\lambda(z) = \frac{n(n+1)\Gamma(n)}{\hat{\tau}\sqrt{\pi}\Gamma(n+\frac{3}{2})}\left(1 - \frac{r^2}{\hat{\tau}^2}\right)^{n+\frac{1}{2}} \qquad 0 < |z| < \hat{\tau} \tag{21}$$

.

2.2 The inverse Abel transformation: from the line density to the amplitude distribution

Since the line density $\lambda(z)$ is what one can normally measure (e.g. in a "tomoscope"), it is interesting to perform the inverse transformation. No information is lost as long as the distribution is circularly symmetric in phase space and $g(r)$ drops to zero faster than $1/r$. The inverse Abel transformation is given by

$$g(r) = -\frac{1}{\pi}\int_r^\tau \frac{d\lambda(z)}{dz}\frac{dz}{\sqrt{z^2-r^2}}\ . \tag{22}$$

As an example, we choose Sacherer's smooth-function line density (19) and prove that we recover the original amplitude distribution (19), namely

$$\begin{aligned}
\text{from} \lambda(z) &= \frac{16}{5\pi\hat{\tau}}\left(1-\frac{z^2}{\hat{\tau}^2}\right)^{5/2} \\
\text{via} \frac{d\lambda(z)}{dz} &= -\frac{16z}{\pi\hat{\tau}}(1-\frac{z^2}{\hat{\tau}^2})^{3/2} \\
\text{we find} g(r) &= -\frac{1}{\pi}\int_r^{\hat{\tau}} \frac{d\lambda(z)}{dz}\frac{dz}{\sqrt{z^2-r^2}} = \frac{3}{\pi\hat{\tau}^2}\left(1-\frac{r^2}{\hat{\tau}^2}\right)^2
\end{aligned}$$

and the smooth function (18) is recovered.

We have presented this technique here, including both the direct transform and its inverse, since we will later attempt to search for an amplitude distribution that correctly models realistic flat bunches. In one approach, the generalized parabolic-like distribution (20) with properly chosen n will be used, and in a second approach a flat function $\lambda(z)$ with its corresponding inverse Abel transform for $g(r)$.

2.3 Flat bunches using parabolic-like distributions

Flat bunches are produced in the PS Booster using different techniques [9]. To correctly describe longitudinal instabilities of such beams, a phase-space distribution has to be chosen, so that its line density resembles that of a flattened bunch.

Making use of the previous analysis, we can proceed by assuming different values of n and observing how as n gets larger, the distribution becomes more packed around the origin. On the other hand and conversely, the line density or projection onto the axis $\lambda(z)$ becomes flatter as n gets smaller.

in particular, by setting $\frac{d\lambda}{dn}| = 0$, we find that for the specific value $n = -1/2$ a perfectly flat line density is obtained. This, however, presents a problem in the phase-space distribution $g(r)$, because for this value of n the latter goes to infinity at the bunch-edge. Introducing a small additional term in $n \pm\epsilon$ removes the singularity. In the example of Fig. 4, the parameter n has been set to $n = -0.49$.

2.4 Flat bunches using the inverse Abel transformation

As suggested by M. Furman in [10] a "flat" longitudinal profile is specified by the line density

$$\lambda(z) = K(1-|z/a|^{1/p})^q \quad |z| < a, p, q \geq 0\ , \tag{23}$$

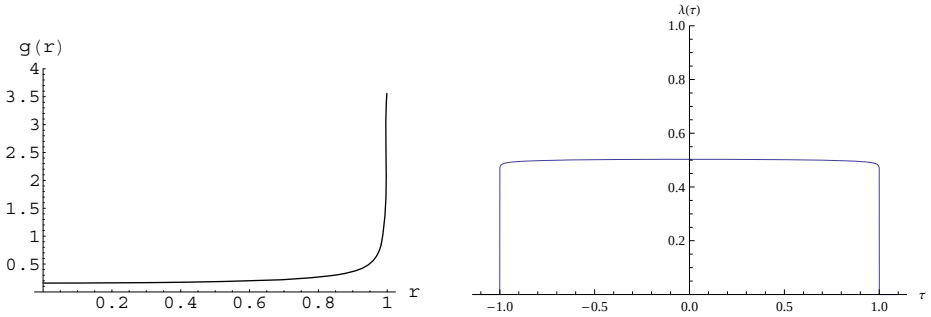

Figure 4: General parabolic-like distribution (20) with $n = -0.49$ and its nearly flat projection onto the time axis, $\lambda(z)$.

where K is a normalization constant. This distribution has a full width of $2a$. A reasonable description of a flat bunch, according to [10], is given by the following choice of parameters: $a = 1$, $p = 0.039$ and $q = 10$. With the corresponding normalization and again choosing $\hat{\tau} = 1$, (23) simplifies to:

$$\lambda(z) = 0.561466 \left(1 - |z|^{25}\right)^{10} \quad . \tag{24}$$

The inverse Abel transformation cannot be given analytically. However, its numerical computation is straightforward. Both the amplitude distribution and its projection are plotted in Fig. 5.

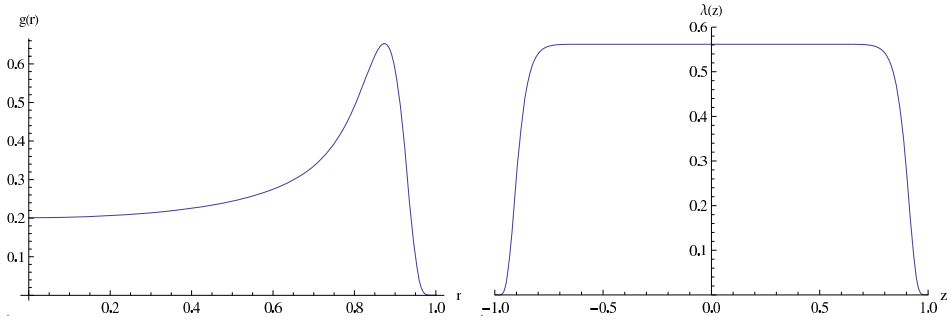

Figure 5: Amplitude distribution $g(r)$ for a flat line density $\lambda(z)$

2.5 Comparison between different distributions

Figure 6 compares different radial distributions obtained from (20) by choosing different exponents n, and the corresponding projections onto the real coordinate z,

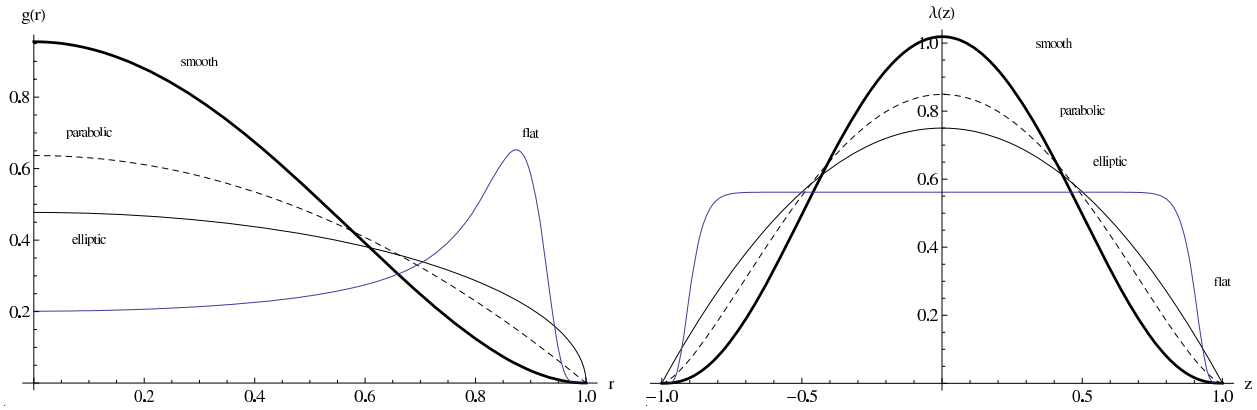

Figure 6: Different distributions of phase space amplitude from (20) with various exponents n [left], and their projections [right], all superimposed.

3 Landau stability diagrams

In the following section, we discuss stability diagrams for different distributions.

3.1 Stability diagrams for parabolic-like distributions

The Sacherer dispersion relation has an analytic solution for the general distribution given by (20).

The dispersion relation in this case reads

$$1 = \frac{\Delta\omega_m}{W_m} \int_0^\infty \frac{r^{2m}}{\Omega - m\omega_{sc}(r)} \cdot \frac{dg_0(r)}{dr} dr \ , \tag{25}$$

where

$$W_m = \int_0^\infty r^{2m} \frac{dg_0(r)}{dr} dr \ . \tag{26}$$

In the absence of incoherent frequency spread ($S = 0$), oscillations about the stationary distribution $g_0(r)$ occur at a frequency of $\Omega = m\omega_{sc0} + \Delta\omega_m$, where, as before, ω_{sc0} denotes the incoherent synchrotron frequency at the centre of the bunch including self forces. The dynamic part of the mth azimuthal coherent frequency shift is defined as $\Delta\omega_m = \Omega - m\omega_{sc0}$. From the discussion of the frequency shift in Appendix A the small amplitude approximation is valid and $\omega_{sc}(r) = (\omega_{sc0} - Sr^2)$. To simplify the integral, we make the following change of variable $u = r^2$. The dispersion relation can then be rewritten as

$$1 = \frac{\Delta\omega_m}{W_m} \int_0^\infty \frac{u^m}{\Omega - m\omega_{sc0} + mSu} \cdot \frac{dg_0(u)}{du} du \ . \tag{27}$$

Eq. (27) includes only the frequency spread from the nonlinearity of the external rf and ignores additional contributions to (or reductions from) the freqeuncy spread that arise from the self force. In other words, we are implicitly making the assumption that the spread introduced by the self fields is either small compared with the external spread or that it also has a quadratic dependence on the amplitude of the synchrotron motion r.

It now is convenient to take S and m out of the integral and to define $z = (\omega_{sc0} - \Omega/m)/S$, so that (27) becomes

$$1 = \frac{\Delta\omega_m}{mSW_m} \int_0^\infty \frac{u^m \cdot \frac{dg_0(u)}{du}}{u - z} du \ . \tag{28}$$

For parabolic-like distributions, written as a function of u as

$$g_0(u) = \frac{n+1}{\pi\hat{\tau}^2} \left(1 - \frac{u}{\hat{\tau}^2}\right)^n \qquad 0 < u < \hat{\tau}^2 \ , \tag{29}$$

the integral assumes the form of a hypergeometric function. Using its properties and that of the Gamma function (a thorough derivation is deferred to subsection 3.2), the dispersion relation yields

$$1 = -\frac{\Delta\omega_m}{mS} \frac{\hat{\tau}^2}{z} {}_2F_1\left(1, 1+m; 1+m+n; \frac{\hat{\tau}^2}{z}\right) \ . \tag{30}$$

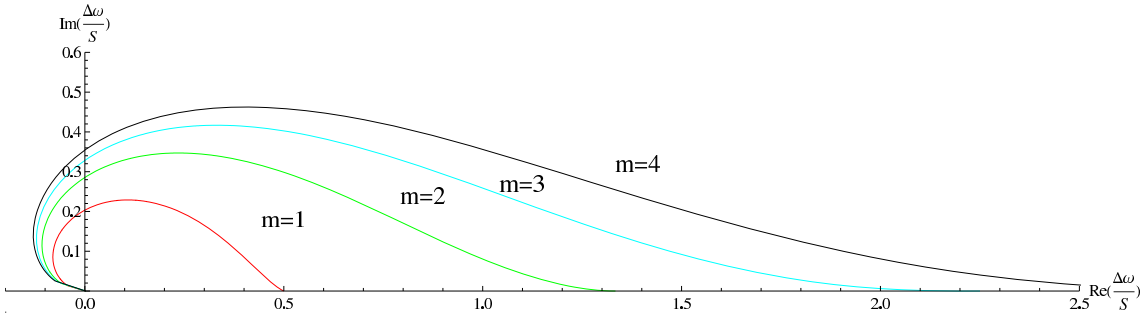

Figure 7: Landau stability diagram for a parabolic-like distribution (20) with $n = 1$, i.e. parabolic distribution $g(r) = \frac{2}{\pi}(1 - r^2)$. Plotted is $\mathrm{Im}(\Delta\omega/S)$ as a function of $\mathrm{Re}(\Delta\omega/S)$ at the border of instability, where $\Delta\omega \equiv \Delta\omega_m$ denotes the dynamic part of the coherent frequency shift in the absence of incoherent frequency spread.

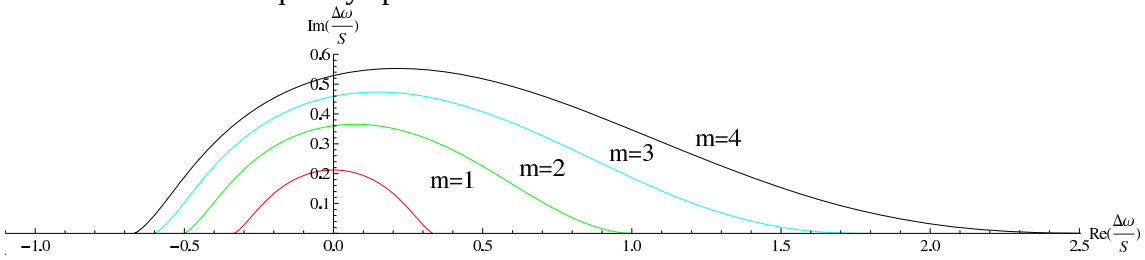

Figure 8: Landau stability diagram for a parabolic-like distribution (20) with n=2, i.e. Sacherer's smooth function $g(r) = \frac{3}{\pi}(1 - r^2)^2$

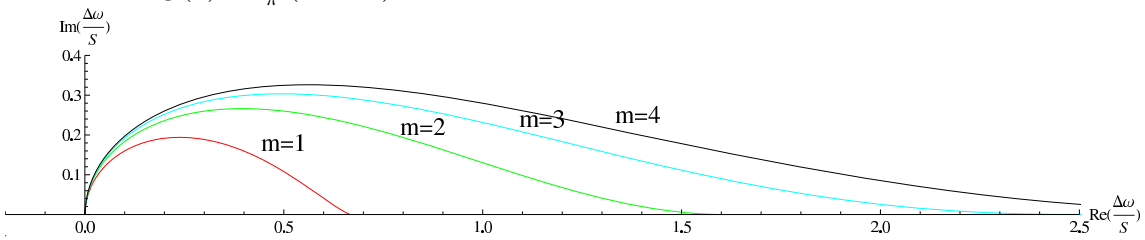

Figure 9: Landau stability diagram for a parabolic-like distribution (20) with n=1/2, i.e. elliptic distribution $g(r) = \frac{3}{2\pi}\sqrt{1 - r^2}$. Plotted is $\mathrm{Im}(\Delta\omega/S)$ as a function of $\mathrm{Re}(\Delta\omega/S)$ at the border of instability, where $\Delta\omega \equiv \Delta\omega_m$ denotes the dynamic part of the coherent frequency shift in the absence of incoherent frequency spread.

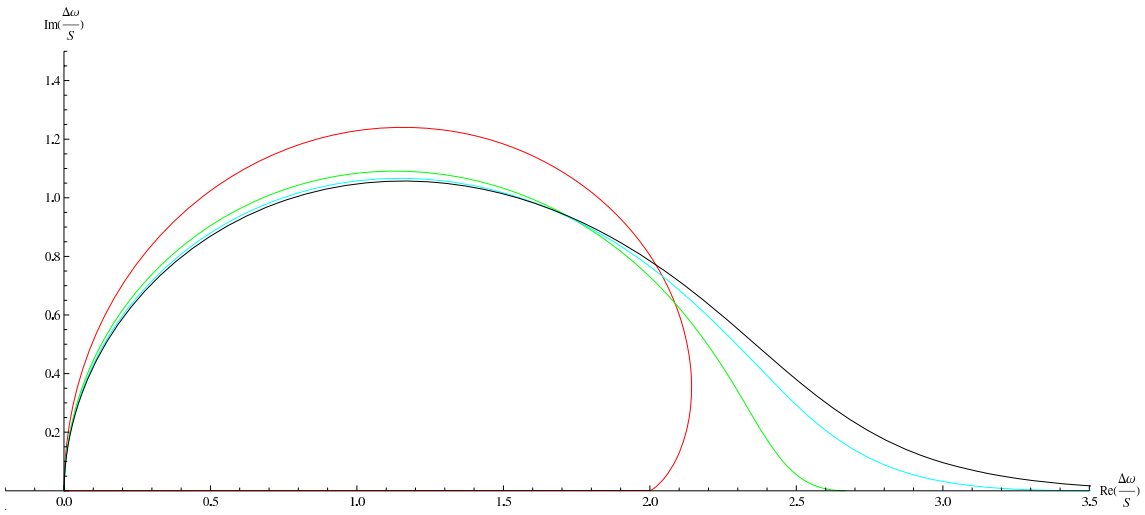

Figure 10: Landau stability diagram for a parabolic-like distribution n=-1/2, i.e. flattest $\lambda(z)$ $g(r) = \frac{1}{2\pi}(1-r^2)^{-\frac{1}{2}}$. Plotted is $\mathrm{Im}(\Delta\omega/S)$ as a function of $\mathrm{Re}(\Delta\omega/S)$ at the border of instability, where $\Delta\omega \equiv \Delta\omega_m$ denotes the dynamic part of the coherent frequency shift in the absence of incoherent frequency spread.

For convenience, we now again choose $\hat{\tau} = 1$, since it is easy to add the correct normalization later, using dimensional arguments. The stability diagram can be plotted by letting z adopt real values between 0 and 1. Examples for $n = 1$, 2, $1/2$ and $-1/2$ are presented in Figs. 7 to 10.

Figures 11, 12, and 13 show the same stability diagrams, but now comparing different distributions for the same azimuthal mode from $m = 1$ to $m = 3$. .

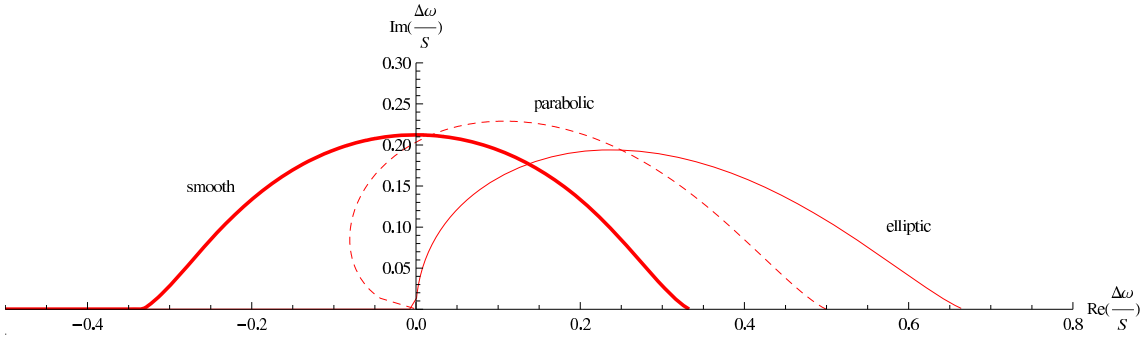

Figure 11: Landau stability diagram for the dipole mode $m = 1$ considering a parabolic, elliptic and smooth distribution. Plotted is $\mathrm{Im}(\Delta\omega/S)$ as a function of $\mathrm{Re}(\Delta\omega/S)$ at the border of instability, where $\Delta\omega \equiv \Delta\omega_1$ denotes the dynamic part of the coherent frequency shift of the rigid dipole mode in the absence of incoherent frequency spread.

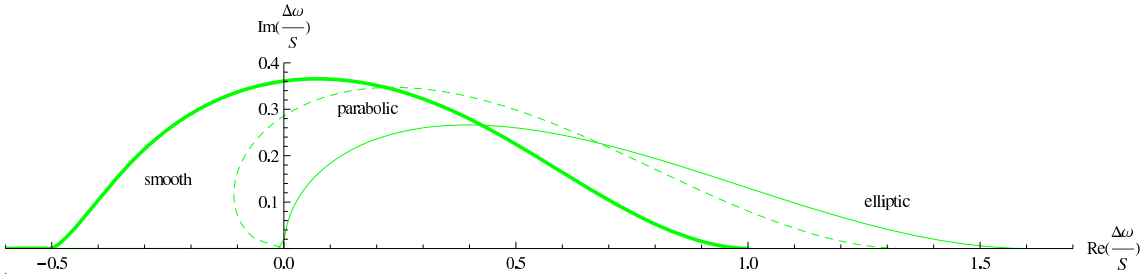

Figure 12: Landau stability diagram for a parabolic, elliptic and smooth distributions corresponding to the quadrupole mode $m = 2$. Plotted is $\mathrm{Im}(\Delta\omega/S)$ as a function of $\mathrm{Re}(\Delta\omega/S)$ at the border of instability, where $\Delta\omega \equiv \Delta\omega_2$ denotes the dynamic part of the coherent frequency shift of the rigid quadrupole mode in the absence of incoherent frequency spread.

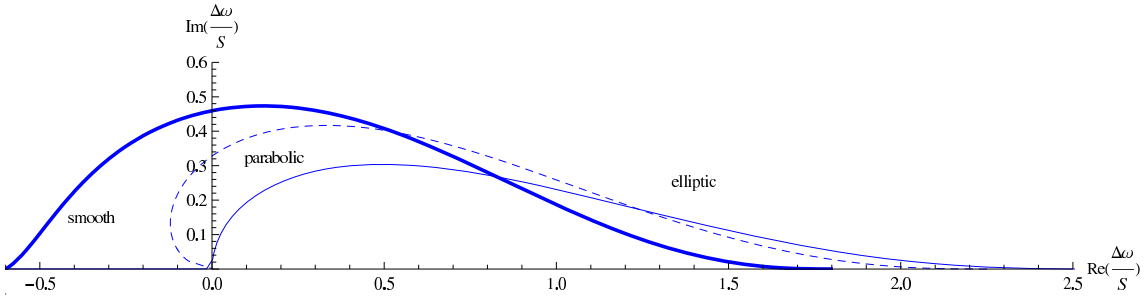

Figure 13: Landau stability diagram for a parabolic, elliptic and smooth distributions corresponding to the sextupole mode $m = 3$. Plotted is $\mathrm{Im}(\Delta\omega/S)$ as a function of $\mathrm{Re}(\Delta\omega/S)$ at the border of instability, where $\Delta\omega \equiv \Delta\omega_3$ denotes the dynamic part of the coherent frequency shift of the rigid sextupole mode in the absence of incoherent frequency spread.

3.2 Solution of Sacherer dispersion relation in terms of Hypergeometric function

The hypergeometric function can be defined as

$$ {}_2F_1(a,b;c;x) = \frac{\Gamma(c)}{\Gamma(b)\Gamma(c-b)} \int_0^1 \frac{t^{b-1}(1-t)^{c-b-1}}{(1-tx)^a} dt \ . \tag{31} $$

Combining (28) and (29) we have

$$ 1 = \frac{\Delta\omega_m}{mSW_m} \int_0^\infty \frac{u^m \cdot \frac{dg_0(u)}{du}}{u-z} du = \frac{\Delta\omega_m}{mSW_m} \frac{-n(n+1)}{z\pi} \int_0^1 \frac{u^m \cdot (1-u)^{n-1}}{-(1-\frac{u}{z})} du \ , \tag{32} $$

and comparing (31) and (32), we can easily identify coefficients term by term,

$$ \begin{aligned} a &= 1 \ , \\ b &= 1+m \ , \\ c &= 1+m+n \ , \\ x &= \frac{1}{z} \ , \end{aligned} $$

so that (32) can be rewritten as

$$ 1 = \frac{\Delta\omega_m}{SW_m} \frac{n(n+1)}{z\pi m} \frac{\Gamma(1+m)\Gamma(n)}{\Gamma(1+m+n)} {}_2F_1\left(1, 1+m; 1+m+n; \frac{1}{z}\right) \ . \tag{33} $$

The coefficient W_m can be computed in a similar fashion, after setting $a = 0$. Since ${}_2F_1(0, 1+m; 1+m+n; 1/z) = 1$ we obtain

$$ W_m = \frac{-n(n+1)}{\pi} \frac{\Gamma(1+m)\Gamma(n)}{\Gamma(1+m+n)} \ . \tag{34} $$

Hence, the dispersion relation (33) simplifies to

$$ 1 = -\frac{\Delta\omega_m}{mS} \frac{1}{z} {}_2F_1(1, 1+m; 1+m+n; \frac{1}{z}) \ , \tag{35} $$

which is our Eq. (30).

3.3 Sign convention

3.3.1 Real part of $\Delta\omega_m$

Depending on the convention that has been chosen, $e^{j\Omega t}$ (engineering convention), or $e^{-i\Omega t}$, the shape of the stability diagram will be flipped around the imaginary axis. A fundamental question arises when asked to relate the frequency shift with the impedance.

Not only is it relevant what choice of the sign has been made, but it is also necessary to determine whether the beam is driven by a *space-charge (capacitive) impedance below transition* or by an *inductive impedance below transition*. According to A. Hofmann, to avoid confusion, accelerator physicists use causality arguments when discussing stability diagrams. For example, if we are dealing with space charge below transition where stability will be lost when $\Delta\omega_m$ reaches its peak, i.e. for $z = 0$ (see the subsequent discussion in subsection 3.4), we then know that this point should be on the half plane where $\mathbb{R}e(\Delta\omega_m) > 0$.

3.3.2 IMAGINARY PART OF $\Delta\omega_m$

Using Cauchy's theorem it is possible to separate the previous integral into two parts: the principal value and a residuum:

$$\int \frac{F(x)}{x - x_0 \mp \imath\epsilon} dx = \mathcal{PV} \int \frac{F(x)}{x - x_0 \mp \imath\epsilon} dx \pm \imath\pi F(x_0) \tag{36}$$

Introducing this mathematical fact into the dispersion relation yields

$$1 = \frac{\Delta\omega_m}{S} \int_0^1 \frac{F(u)}{u - z \mp \imath\epsilon} du = \frac{\Delta\omega_m}{S} \left(I(z) \pm \imath\pi F(z) \right) \ , \tag{37}$$

where

$$I(z) = \mathcal{PV} \int \frac{F(x)}{x - x_0} dx \ ,$$

and, in our case,

$$F(u) = \frac{u^m g'(u)}{m W_m} \ .$$

The computation of I and F for a parabolic-like distribution (20) is straightforward:

$$\begin{aligned} I(z) &= -\mathbb{R}e \left(\frac{1}{z} {}_2F_1 \left(1, 1 + |m|, 1 + |m| + n, \frac{1}{z} \right) \right) \ , \\ F(u) &= \left(\frac{u}{m} \right)^m \left(1 - \frac{u}{m} \right)^{n-1} \frac{\Gamma(1 + m + n)}{m\Gamma(n)\Gamma(1 + m)} \ . \end{aligned}$$

An important matter regarding the sign of the imaginary part arises here. The hypergeometric function has a branch line from $z = \infty$ to $z = 1$. So the analytic continuation is at choice. By introducing $\imath\epsilon$ with $\epsilon > 0$, z approaches the axis from above and we make sure that causality is fulfilled. For the sake of consistency, it will be assumed that a force of the form $e^{-i\Omega t}$ drives the beam and by choosing $\Omega - > \Omega + \imath\epsilon$, it is a force that grows with time at an infinitesimal rate as $e^{-i\Omega t + \epsilon t}$. So all points on the negative half-plane of the stability diagram will be automatically damped. It is only in the upper half plane, $\mathbb{I}m(\Delta\omega_m) > 0$, that Landau damping can actually happen.

Figure 3.3.2 shows $\mathbb{R}e(\Delta\omega_m)$ and $\mathbb{I}m(\Delta\omega_m)$ as functions of real values z, describing the threshold of instability. Note that the Landau-damped region corresponds to $z\epsilon[0, 1]$. In addition, the difference between choosing $+\imath\epsilon$ and $-\imath\epsilon$ is indicated by the two graphs.

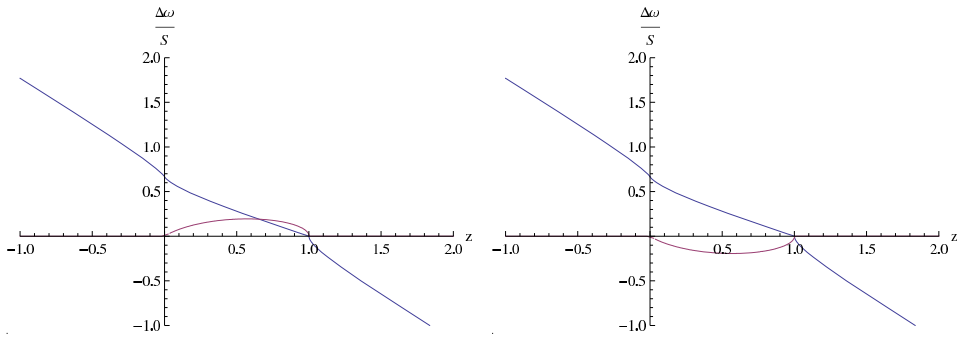

Figure 14: $\mathbb{R}e(\Delta\omega_m)$ and $\mathbb{I}m(\Delta\omega_m)$ vs. z for $+\imath\epsilon$ and $-\imath\epsilon$, respectively. The graph corresponds to $n = 1/2$ (elliptic distribution) and $m = 1$ (dipole mode).

3.4 General method for calculating the intensity threshold

Landau damping is lost when the coherent frequency Ω lies outside the band of incoherent synchrotron frequencies. The corresponding threshold intensity for the case of a purely capacitive space-charge impedance can be calculated from

$$\Omega = m\omega_{sc}^{min} \quad \text{or} \quad \Omega = m\omega_{sc}^{max} \ ,$$

with ω_{sc}^{min} (ω_{sc}^{max}) denoting the minimum (maximum) synchrotron frequency inside the bunch and m representing the azimuthal mode number. The first case applies for an inductive impedance below transition, where the synchrotron frequencies are shifted upwards with increasing bunch intensity. Here the threshold intensity is determined by the lowest synchrotron frequency. The second case applies for a space-charge (capacitive) impedance below transition (or an inductive impedance above transition), and where the threshold intensity is determined by the highest synchrotron frequency.

This can easily be justified by taking a close look at the *Sacherer formula* that relates the dynamical coherent frequency shift with the intensity and impedance [11, 12] [3]

$$\Delta\omega_m = -\imath\frac{m\omega_{sc}}{m+1}\frac{I_b}{3B^3V_t h\cos\phi_s}\left(\frac{Z}{n}\right)_{eff} \ . \tag{38}$$

where B is the bunching factor, defined as $B = \tau_b f_0$ with τ_b the total bunch-length in seconds. By definition $\cos\phi_s > 0$ below transition and $\cos\phi_s < 0$ above transition. The parameter V_t denotes the total peak voltage, h the harmonic number and Z_{eff} the effective impedance. For a positive capacitive impedance below transition we have $\mathbb{R}e(\Delta\omega_m) > 0$.

The incoherent frequency shift due to self-forces (already included in ω_{sc}) for a parabolic line distribution (or elliptical density distribution) is given by [4]:

$$\Delta\omega_{incoh} = -\eta\frac{3e^2N_b}{8\pi\beta^2E_0\omega_{s0}\hat{\tau}^3}\mathbb{I}m(Z_0/n) \tag{39}$$

[3] Neither Sacherer nor Zotter give any hint for which type of distribution this formula applies, but possibly it has been derived for a parabolic line density. In the future we need to verify whether or not this formula is a reasonable approximation for other distributions, and in particular for flat profiles.

Summarizing, for space-charge below transition the incoherent frequency is shifted *downwards*, $\Delta\omega_{incoh} < 0$ and the bunch as a whole is coherently shifted *upwards*, $\mathbb{R}e(\Delta\omega_m) > 0$. Figure 15 illustrates this process.

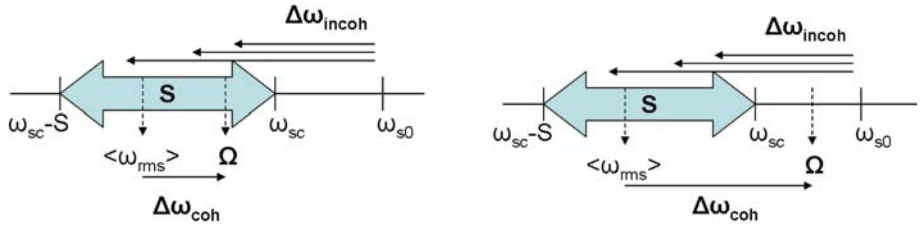

Figure 15: Graphical representation of a capacitive impedance below transition with rms frequency spread $< \omega_{rms} > \stackrel{!}{\equiv} \omega_{sc0}$. The left diagram shows a case where Landau damping occurs, because the coherent tune shift falls within the frequency spread $\Delta\omega_m/S < 1$. The diagram on the right shows the case of $\Delta\omega_m/S >> 1$, where no Landau damping occurs.

3.4.1 THRESHOLD VALUE OF $\frac{\Delta\omega_m}{S}$ FOR ANY $g(r)$ DISTRIBUTION

We note that the condition $\Omega = m\omega_s^{max}$ translates into $z = 0$, where we define z as in (28),

$$z = \frac{\omega_{sc0} - \Omega/m}{S} \ . \tag{40}$$

A general recipe for the calculation of the threshold intensity can now be given:

1. For any given distribution in longitudinal phase space $g(r)$ calculate its derivative $\frac{dg(r)}{dr}$.
2. Define a function
$$F(z,m) = \frac{\int_0^\infty \frac{u^m \cdot \frac{dg_0(u)}{du}}{u-z} du}{\int_0^\infty u^m \cdot \frac{dg_0(u)}{du} du} \ ,$$
where we have changed variables according to $u = r^2$.
3. Evaluate $\frac{\Delta\omega_m}{S}(z,m)|_{z=0} = \frac{1}{F(z,m)}|_{z=0}$
4. Use Sacherer's coherent shift formula 38) plus a good approximation for the frequency spread S, e.g. Eq. (55) in the appendix), to express the result in terms of the intensity:
$$I^m_{threshold} = \imath \frac{m+1}{m} \frac{3\pi^2 B^5 h^3 V_T \cos\phi_s}{16 \cdot \left(\frac{Z}{n}\right)_{eff}} \left[\frac{\Delta\omega_m}{S}\right]_{z=0} \ . \tag{41}$$

We must add two words of caution here. First the "recipe" that is described above is valid only for a capacitive impedance below transition or an inductive impedance above transition; otherwise the evaluation of the dispersion relation should be done for $z = 1$ instead of $z = 0$. Second, depending on the validity range of Sacherer's coherent tune shift formula, the recipe may or may not give a good estimate for an arbitrary distribution. In our following applications, the shape of the distribution enters only through $\Delta\omega_m/S|_{z=0}$.

3.4.2 THRESHOLD VALUE OF $\frac{\Delta\omega_m}{S}$ FOR PARABOLIC LIKE DISTRIBUTIONS

For parabolic-like distributions we already have an expression for $\frac{\Delta\omega_m}{S}$ in terms of the hypergeometric function of second kind:

$$\frac{\Delta\omega_m}{S} = -\lim_{z\to 0} \frac{mz}{{}_2F_1(1, 1+m; 1+m+n; \frac{1}{z})} \,. \tag{42}$$

Results for the four lowest order modes and four different parabolic-like distributions of the type (20), differing in the value of n, are compiled in Table 1.

Table 1: Stability limits $\Delta\omega_m/S$ for different distributions (20), characterized by n, and different azimuthal modes, specified by m.

$g(r)$ **distribution**	**n**	$\frac{\Delta\omega_1}{S}$	$\frac{\Delta\omega_2}{S}$	$\frac{\Delta\omega_3}{S}$	$\frac{\Delta\omega_4}{S}$
Smooth	*2*	$1/3$	1	$9/5$	$8/3$
Parabolic	*1*	$1/2$	$4/3$	$9/4$	$16/5$
Elliptic	*1/2*	$2/3$	$8/5$	$18/7$	$32/9$
Flat	*-1/2*	2	$8/3$	$18/5$	$32/7$

A distribution that better describes the flat bunch was given in section (2.2). It is given by the Abel transform of (23). The derivative of $g(r)$ is required for the dispersion relation; this can be calculated numerically by means of the fundamental theorem of calculus and plugged into the integral. We evaluate the integral only at $z = 0$ to obtain the threshold value for $\frac{\Delta\omega_m}{S}$. Table 2 presents the resulting stability limits for Furman's flat distribution (23).

Table 2: Stability limits $\Delta\omega_m/S$ for the Abel transform of Furman's flat line density (23, and different azimuthal modes, specified by m.

$g(r)$ **distribution**	**n**	$\frac{\Delta\omega_1}{S}$	$\frac{\Delta\omega_2}{S}$	$\frac{\Delta\omega_3}{S}$	$\frac{\Delta\omega_4}{S}$
Flat	-	1.5821	2.1293	2.8987	3.7087

The flatter the line density $\lambda(z)$, the more stable the beam is. One of the cures for loss of Landau damping on the transverse plane due to space-charge has been that of flattening the bunch. By increasing the bunching factor considerably (e.g. up to $B_f = 0.55$ in the PS Booster) a decrease of the dynamic coherent shift is obtained, because $\Delta\omega_m \propto 1/B^3$. This may also explain why the more realistic flat bunch distribution has lower threshold values than the flat parabolic-like distribution.

A word of caution may be in order. Not only the stability diagram, but for a given impedance and bunch charge also the coherent tune shift $\Delta\omega_m$ will be different for different beam distributions, with Eq (38) probably being strictly valid only for an elliptic distribution. In addition, Eq. (27) applies only if the frequency spread is dominated by the external rf curvature or for an elliptic distribution $g_0(r)$.

4 Application to the LHC injectors

4.1 Intensity thresholds for the LHC beam in the PS Booster

In the longitudinal plane space charge leads to a reduction of the available bucket area with intensity. It also leads to a loss of Landau damping above a given bunch population, namely, N_{th}.

The PS Booster has three rf systems: C02 ($h = 1$), C04 ($h = 2$ or $h = 4$), and the C16 system capable of producing harmonics from 10 to 27 at 50 MeV. Both C02 and C04 operate at up to 8 kV. At injection, the PSB is normally operated with $h = 1$ as the main harmonic and the $h = 2$ harmonic system is superimposed in anti-phase to provide bunch flattening. The harmonic rf cavities of $h = 2$ or higher will, however, not be considered in the following analysis and the issue of a double rf system will be handled in Appendix A. Table 3 lists the parameters for the standard LHC beam [4].

Table 3: Parameters for LHC beam in the PS Booster.

Normalized emittance for the LHC beam ϵ_N	2.5 μm
Betatron Tunes $Q_{x,y}$ (old working point)	$\approx 4.2, 5.45$
PSB radius	25 m
Beam pipe radius b	35-65 mm (average =50 mm)
Full bunch length $2\hat{\tau}$	750 ns
Revolution frequency f_{rev}	600 kHz
Voltage up to acceleration	8 kV
Momentum compaction factor α	0.0608
$\lvert\eta\rvert$	0.8411

For the kinetic energy at injection (50 MeV) we have $\gamma = 1.053 \approx 1$ and $\beta = 0.31$. The capacitive (or negative inductive) impedance due to longitudinal space charge is given by

$$\frac{Z_{sc}}{n} = \imath \frac{gZ_0}{2\beta\gamma^2} = \imath \frac{376.73\Omega \cdot g}{2\beta\gamma^2} \ . \ , \tag{43}$$

where $Z_0 = 376.73\ \Omega$ is the vacuum impedance and g a form factor for longitudinal space charge usually written as $g = \frac{1}{2} + 2\ln(b/a)$, with b the beam pipe radius and $a = 2\sigma_x$ twice the rms beam size.

Since for the LHC beam $\epsilon_N = 2.5\mu m$ and $Q \approx 5$, the average transverse beam size is about

$$a = \sqrt{\epsilon_{2\sigma}\frac{R}{Q}} = \sqrt{\frac{4\epsilon_N\beta_{av}}{\beta\gamma}} = \sqrt{\frac{4 \cdot 2.5 \cdot 10^{-6} \cdot 5}{0.3}} = 0.0129\ \mathrm{m} = 12.91\ \mathrm{mm} \ . \tag{44}$$

The value of the form factor is given by

$$g = \frac{1}{2} + 2\ln b/a = \frac{1}{2} + 2\ln\frac{50}{12.91} \approx 3.20804 \ . \tag{45}$$

[4] Information provided by Dr. M. Chanel.

The bunching factor for a single bunch can be calculated as $B = f_{rev} 2\hat{\tau} = 9/20$. Assuming a synchronous phase equal zero, $\phi_s = 0$, the frequency spread is given by $S = \frac{\pi^2}{16} B^2 \omega_s = 0.124912\omega_s$ (see Eq. (55) below). The peak voltage is $V_t = 8kV$, the harmonic number is $h = 1$ and *below transition* we have $\cos\phi_s = 1$. We now apply (41)

$$I^m_{threshold} = \imath \frac{m+1}{m} \frac{3\pi^2 B^5 h^3 V_T \cos\phi_s}{16 \cdot \left(\frac{Z}{n}\right)_{eff}} \left[\frac{\Delta\omega_m}{S}\right]_{z=0} = 0.147572 \frac{m+1}{m} \left[\frac{\Delta\omega_m}{S}\right]_{z=0} \text{ A} , \quad (46)$$

which corresponds to a total threshold bunch intensity above which Landau damping would be lost and hence, give rise to instabilities, of

$$N_{th} = \frac{0.147572 \frac{m+1}{m} \left[\frac{\Delta\omega_m}{S}\right]_{z=0} \cdot}{e \cdot f_{rev}} \approx 1.53 \cdot 10^{12} \frac{m+1}{m} \left[\frac{\Delta\omega_m}{S}\right]_{z=0} . \quad (47)$$

This total booster intensity is later divided into 12 bunches that will be fed to the LHC, so that in terms of the LHC intensity we have the equivalent threshold

$$N^m_{th,LHC} \approx 1.28 \cdot 10^{11} \frac{m+1}{m} \left[\frac{\Delta\omega_m}{S}\right]_{z=0} ppb \quad (48)$$

The nominal LHC bunch intensity is 1.15×10^{11} protons. Table 4 lists the threshold values for various distributions and azimuthal modes.

Table 4: Equivalent LHC threshold bunch intensities due to loss of longitudinal Landau damping in the PS booster, for different beam distributions and modes.

$g(r)$ **distribution**	**n**	$N^{m=1}_{th,LHC}(10^{11})$	$N^{m=2}_{th,LHC}$	$N^{m=3}_{th,LHC}$	$N^{m=4}_{th,LHC}$
Smooth	*2*	0.85	**1.92**	**3.07**	**4.26**
Parabolic	*1*	1.28	**2.56**	**3.84**	**5.12**
Elliptic	*1/2*	**1.70**	**3.07**	**4.38**	**5.68**
Flat	*-1/2*	**5.12**	**5.12**	**6.14**	**7.31**
Flat + Tail	-	**4.05**	**4.08**	**4.94**	**5.93**

These results indicate that in case of the nominal LHC beam Landau damping might be lost only for the dipole mode. The PSB is equipped with an rf phase loop mechanism on the $h = 1$ rf system which suppresses any dipole mode instabilities. In principle, loss of Landau damping for higher modes could lead to beam losses at injection. However, Table 4 demonstrates that in the PS Booster the azimuthal modes higher than the dipole mode become unstable only at bunch intensities much higher than nominal, and indeed even higher than the so-called ultimate LHC bunch intensity of 1.7×10^{11} protons per bunch.

Our above analysis has neglected the existence of the double rf system plus the additional cavity that is used for longitudinal blow up.

4.2 Intensity thresholds for the LHC beam in the SPS

Table 5 lists key parameters for the LHC beam at injection into the SPS (26 GeV).

Table 5: Parameters of the LHC beam at injection into the SPS.

Horizontal normalized r.m.s. emittance ϵ_N^H	2.5 ± 0.3 μm
Vertical normalized r.m.s. emittance ϵ_N^V	3.0 ± 0.3 μm
Longitudinal normalized emittance (2σ) ϵ_N^z	0.25 $eV \cdot s$
Betatron Tunes $Q_{x,y}$	26.13, 26.19
SPS circumference	6.9 km
Beam pipe radius b	37.4-43 mm
Bunch length	$4.2\pm$0.1 ns (at 4σ)
Revolution frequency f_{rev}	43.450 kHz
Voltage up to acceleration	from 2 to 3 MV
Momentum compaction factor α	0.00192
$\lvert\eta\rvert$	$5.98 \cdot 10^{-4}$

We proceed in the same way as before, but we now take into account only the inductive impedance, since space charge is negligible. For kinetic energy at injection (26 GeV) we have $\gamma \approx 26$ and $\beta = 0.99$. The recently measured value of the longitudinal inductive impedance in the SPS (2007) is approximately [13]

$$\frac{Z_{ind}}{n} \approx -\imath 10\Omega \; . \tag{49}$$

The bunching factor for a single bunch is given by $B = f_{rev} 2\hat{\tau} = 1.825 \times 10^{-4}$. The peak voltage is $V_t = 2000$ kV, the harmonic number is $h = 4620$, and *above transition* we have $\cos\phi_s = -1$. We again apply (41),

$$I^m_{threshold} = \imath \frac{m+1}{m} \frac{3\pi^2 B^5 h^3 V_T \cos\phi_s}{16 \cdot \left(\frac{Z}{n}\right)_{eff}} \left[\frac{\Delta\omega_m}{S}\right]_{z=0} = 0.00734 \frac{m+1}{m} \left[\frac{\Delta\omega_m}{S}\right]_{z=0} A/bunch \; , \tag{50}$$

and the threshold population is given by

$$N_{th} = \frac{0.00734 \frac{m+1}{m} \left[\frac{\Delta\omega_m}{S}\right]_{z=0}}{e \cdot f_{rev}} \approx 1.054 \cdot 10^{12} \frac{m+1}{m} \left[\frac{\Delta\omega_m}{S}\right]_{z=0} \text{ ppb} \; . \tag{51}$$

The nominal intensity per bunch is $1.15 \times 10^{11} ppb$. Table 6 lists the threshold values for various distributions and azimuthal modes.

Table 6: Threshold LHC bunch intensities due to loss of Landau damping in the SPS, for different beam distributions and modes.

$g(r)$ **distribution**	**n**	$N_{th}^{m=1}$**(**10^{12}**)**	$N_{th}^{m=2}$	$N_{th}^{m=3}$	$N_{th}^{m=4}$
Smooth	*2*	**0.70**	**1.58**	**2.52**	**3.51**
Parabolic	*1*	**1.05**	**2.10**	**3.16**	**4.21**
Elliptic	*1/2*	**1.40**	**2.52**	**3.61**	**4.68**
Flat	*-1/2*	**4.21**	**4.21**	**5.05**	**6.02**
Flat + Tail	-	**3.33**	**3.36**	**4.07**	**4.88**

5 Conclusions

A general recipe has been given for the calculation of intensity thresholds in the two cases of a space charge impedance below transition or inductive impedance above transition, respectively, based on the groundbreaking work of Sacherer. Different beam distributions have been considered and flat bunches have proven to be more stable than bunches of other shapes. Non-linearities introduced by a double rf system do not permit a simplification of the Sacherer equation in the same way as it is done for a single harmonic system. Stability diagrams are a useful tool from which approximate values of intensity thresholds can be obtained. The bunch-intensity thresholds where longitudinal Landau damping is lost in the SPS are about 20% lower than the corresponding values for the PS booster. In either accelerator, the lowest thresholds are found for the dipole modes ($m = 1$), which are partially controlled by existing rf feedback loops. However, in the case of a multi-bunch beam, as in the SPS, one cannot damp rigid dipole bunch oscillations of individual bunches with the phase loop, since the latter detects an average phase error over several bunches and corrects ALL bunches for this average error. Landau damping, if lost, can be restored by either increasing the frequency spread S, or by decreasing the frequency shift $\Delta\omega_m$, e.g. via flattening the bunch. Introducing a double rf system increases the frequency spread and is a cure for loss of Landau damping. However, the double rf system is thought to create some other kind of instabilities [14].

For the moment, two open questions remain, namely the implications of the "synthetic kernel" ansatz and the validity range of the Sacherer formula for the coherent tune shift.

6 Acknowledgements

I wish to thank my supervisor Frank Zimmermann and Giovanni Rumolo for their help, interest and encouragement. I have profited from discussions with A. Hofmann, B. Zotter, F. Pedersen, M. Chanel, E. Metral and E. Shaposhnikova, as well as correspondence with K.Y. Ng, leading experts on accelerator physics and instabilities. Thanks go also to Gianluigi Arduini and Frank Zimmermann for a careful reading of the manuscript.

This work was supported by the European Community-Research Infrastructure Activity under the FP6 "Structuring the European Research Area" programme (CARE, contract number RII3-CT-2003-506395).

References

[1] F.J. Sacherer, *A Longitudinal Stability Criterion for Bunched Beams*, CERN report CERN/MPS/BR 73-1,1973; IEEE Trans. Nuclear Sci. NS 20,3,825 (1973)

[2] B. Zotter, *Longitudinal Stability of Bunched Beams Part II: Synchrotron Frequency Spread*, CERN Report CERN SPS/81-19 (D1), 1981

[3] F.J. Sacherer, *Methods for Computing Bunched Beam Instabilities*, CERN report CERN/SI-BR/72-5, 1972

[4] K.Y. Ng, *Comments on Landau Damping due to Synchrotron Frequency Spread*, FERMILAB-FN-0762-AD, 2005

[5] E. Metral, *Longitudinal Bunched-Beam coherent modes: From Stability to instability and inversely*, CERN-AB 2004-002(ABP), 2002

[6] F. Ruggiero, private communication (1997).

[7] P.W. Krempl, *The Abel-type integral transformation and its application to density distributions of particle beams*, MPS/Int.BR/74-1, 1974

[8] F. Ruggiero, J. Berg, *Stability Diagrams for Landau Damping*,Proceedings of the 1997 Particle Accelerator Conference, 1997

[9] C. Carli, M. Chanel, *Creation of hollow bunches by redistribution of phase space surfaces*,Proceedings of EPAC, 2002

[10] M. Furman, *E-Cloud in PS2, PS+, SPS+*, Proceedings LHC-LUMI-06, 2006 Proceedings LHC-LUMI-06.

[11] F.J. Sacherer, *Bunch Lengthening and Microwave Instability*, 1977 PAC Chicago, 1977.

[12] B. Zotter, *Bunch Lengthening and Microwave Instability*, in A.W. Chao and M. Tigner (eds.), *Handbook of Accelerator Physics and Engingeering*, Second Printing, World Scientific, Singapore, 2002, p. 122.

[13] E. Shaposhnikova, *Measurement of the low frequency part of the SPS longitudinal impedance: preliminary results*, CERN APC meeting 03.08.2007

[14] E. Shaposhnikova et al, *Beam transfer functions and beam stabilisation in a double RF system*, PAC 2005 Knoxville, 2005.

[15] P. Bramham, A. Hofmann, P.B. Wilson, *A Higher Harmonic Cavity to Increase the Bunch Length in LEP-70*, Report No. CERN-LEP/70-25, 1970

[16] E. Shaposhnikova et al., *Beam transfer functions and beam stabilization in a double rf system*, CERN-AB-2005-026.

[17] J.M. Baillod, L. Magnani, G. Nassibian, F. Pedersen, W. Weissflog, *A Second Harmonic (6–16 MHz) RF System with Feedback-Reduced Gap Impedance for Accelerating Flat-Topped Bunches in the PS Booster*, 1983 PAC Santa Fe (1983).

[18] O. Boine-Frankenheim et al., *Space charge effects in bunches for different rf wave forms*, PR Accelerators and beams 8, 034201, 2005.

[19] S.Y. Lee, *Accelerator Physics*, 2nd Edition, World Scientific, Singapore, 2004

[20] A.W. Chao, M. Tigner, *Handbook of Accelerator Physics and Engineering*, World Scientific, Singapore, 1999.

[21] F. Pedersen, A. Hofmann, *Bunches with local elliptic energy distributions*, 1979 PAC San Francisco, 1979.

[22] Ahmed M. Al-khateeb, G. Rumolo et al., *Analytical calculation of the longitudinal space charge and resistive wall impedances in a smooth cylindrical pipe*, 2001

A Change of tune with amplitude for single and double rf systems

A.1 Change of tune with amplitude in a single rf system

For a stationary bucket (with zero synchronous phase $\phi_s = 0$) the synchrotron tune change as a function of the amplitude of the synchrotron oscillation r previously defined is given by [19]:

$$\omega_{sc}(r) = \frac{\pi\omega_{sc0}}{2K(\sin(r/2))} \ , \tag{52}$$

where $K(k)$ is the complete elliptic integral of the first kind:

$$K(x) = \int_0^\infty \frac{dw}{\sqrt{1 - x^2 \sin^2 w}} \ . \tag{53}$$

For small amplitude oscillations

$$\omega_{sc}(r) \approx \left(1 - \frac{1}{16} r^2\right) \omega_{sc0} \ . \tag{54}$$

This is of the same form as our approximation (27), namely $\omega_{sc}(r) = (\omega_{sc0} - Sr^2)$, where, however, S is meant to characterize the total frequency spread. We can estimate the latter from (54) as

$$S \approx \frac{\pi^2}{16}(hB)^2\omega_{sc0} \ , \tag{55}$$

where h denotes the harmonic number and B the bunching factor defined as the full bunch duration multiplied by the revolution frequency. The exact dependence of the synchrotron tune on longitudinal amplitude ϕ according to (52) and the approximation (54) are compared in Fig. 16. For completeness, in the general case of an accelerating single-harmonic rf bucket the total frequency spread S along a parabolic bunch is given by [20]:

$$S = \left(1 + \frac{5}{3}\tan^2\phi_s\right) \frac{\pi^2}{16}(hB)^2\omega_{sc0} \ . \tag{56}$$

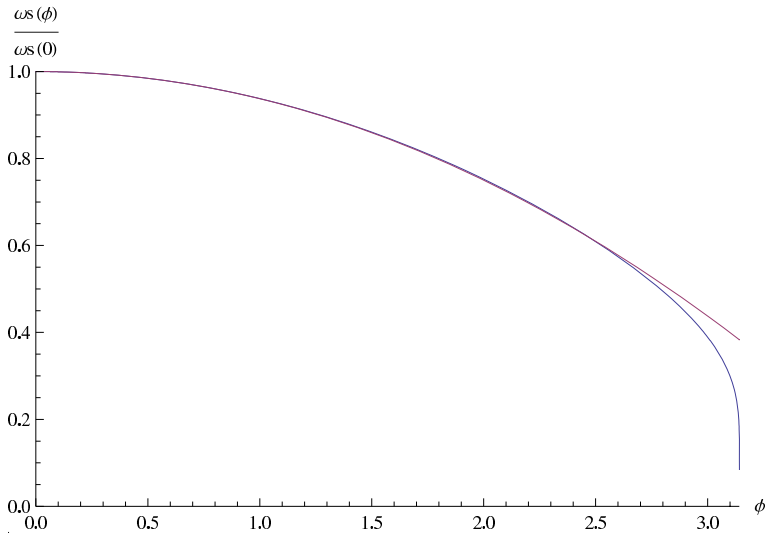

Figure 16: Exact dependence of the synchrotron frequency on the amplitude (52) and the approximation with $S/\omega_{sc0} = 1/16$.

A.2 Change of tune with amplitude in a double rf system

At low or medium energies like in the PS Booster, bunches cannot be regarded as being short relative to rf waves. In other words, the nonlinearity of the rf waves will affect particles of large amplitude. This is true specially for double rf systems.

The main reason for using a double rf system is to flatten the bunch and increase the transverse space charge limit. This, however, will make the motion fully non-linear (see [15]). An analytic approach to the study of the double rf system is possible if the ratio of the voltages is of $1/2$. This has already been suggested by F. Pedersen [17] and studied in detail by E. Shaposhnikova [16]. Other investigations of double rf systems with space-charge effects were performed by O. Boine-Frankenheim at GSI, also for $r = 0.5$ [18]. The PS Booster, however, uses a second harmonic cavity operated with the same voltage as the first harmonic system, i.e. $r = 1$.

A.2.1 Synchrotron equation of motion in a double rf system

For an extensive treatment of single-particle dynamics in a double haromic rf system we refer to S.Y. Lee's Accelerator Physics textbook [19].

We study the case of the PS Booster where $h_1 = 1$ and $h_2 = 2$, hence $h = \frac{h_2}{h_1} = 2$. To simplify the discussion, only stationary buckets are considered. Using the normalized coordinates $(\phi, \mathcal{P} \equiv \dot{\phi}/\nu_s)$ the Hamiltonian is

$$H = \frac{1}{2}\nu_s \mathcal{P}^2 + \nu_s \left[(1 - \cos\phi - \frac{r}{2}(1 - \cos 2\phi))\right] \ , \tag{57}$$

where $r = -V_2/V_1$ (the minus sign accounts for the fact that the cavities are out of phase as in the PSB). Using action-angle variables and defining $\hat{\phi}$ as the maximum phase angle for a given Hamiltonian torus of energy E the synchrotron tune is expressed by

$$\frac{\omega_s(\hat{\phi})}{\omega_s(0)} = \frac{\pi\sqrt{(1-2r) + 2t^2 + (1+2r)t^4}}{2(1+t^2)K(k_1)} \ , \tag{58}$$

where $t = \tan(\hat{\phi}/2)$, K is the elliptic integral of the first kind with modulus

$$k_1 = \frac{t\sqrt{1 + (1+2r)t^2}}{\sqrt{(1-2r) + 2t^2 + (1+2r)t^4}} \ . \tag{59}$$

This formula is valid when $r \leq 0.5$ and it is as well valid for $r > 0.5$ in the range $\phi > \phi_b$, where ϕ_b denotes the intercept of the inner separatrix with the phase axis.

For $r > 0.5$ when $\hat{\phi} < \phi_b$ the normalized synchrotron tune is given by a different expression:

$$\frac{\omega_s(\hat{\phi})}{\omega_s(0)} = \frac{\sqrt{2r}\pi t}{\sqrt{(1+t^2)(1+t_l^2)}} \frac{1}{K(k_2)} \ , \tag{60}$$

with modulus $k_2 = \sqrt{t^2 - t_l^2}/t^2$ and $t_l = \tan(\hat{\phi}_l/2)$, where $\phi_l = 2\arcsin\sqrt{\sin^2(\phi_b/2) - \sin^2(\phi/2)}$. Reading off from the Hamiltonian, the inner separatrix, which passes through the origin, intersects the phase axis at $\pm\phi_b$ with $\cos(\phi_b/2) = 1/\sqrt{2r}$.

A.2.2 R=1 IN THE PS BOOSTER

At injection the beam is accelerated up to 8 kV using both cavities. For $r = 1$ an unstable fixed point exists at the center of as can be seen in the tomograph. Figure 17 shows the variation of the normalized synchrotron frequency with amplitude for $r = 1$ and $r = 0.5$ and $r = 0$ (single rf cavity). The case $r = 1$ exhibits a large discontunity at $\phi = \pi/2$.

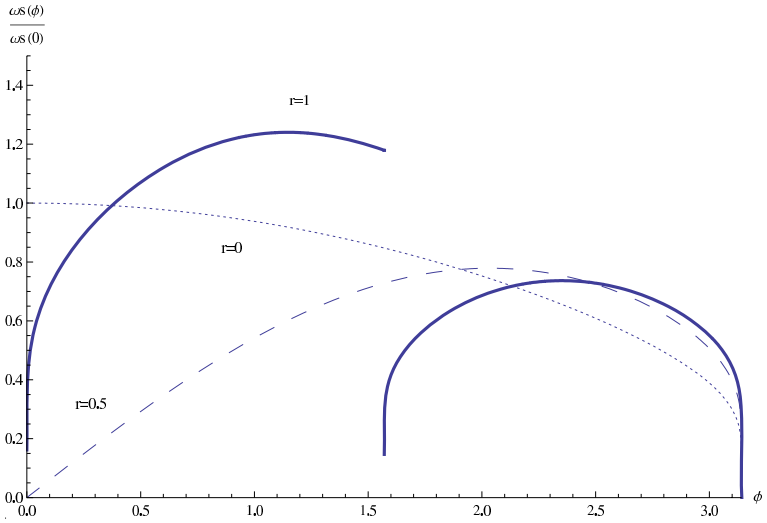

Figure 17: Exact dependence of the synchrotron frequency on the amplitude for a double harmonic rf system with three different values of the second-to-first harmonic voltage ratio r, and for comparison the quadratic approximation for a single harmonic system $\omega_s(r) = (\omega_{s0} - Sr^2)$ with $S/\omega_{s0} = 1/16$.

B Hofmann-Pedersen formalism

In an attempt to obtain results similar to those presented in this paper, the Hofmann-Pedersen formalism has been introduced [21], where bunches with a local elliptic energy distributions are considered, namely the particle distribution as a function of energy is taken to be $g(\phi) = (c/\omega_0)\sqrt{\Delta E_b^2(\phi) - \Delta E^2}$, where $E_b(\phi)$ is the local bunch boundary. This distribution fits well to distributions observed experimentally in proton synchrotron and it enables several analytical calculations. In particular, the self forces caused by space charge and by the inductive wall impedance are proportional to the external focusing force from the rf.

For stationary buckets, (32) in [21] may be used to compute the threshold intensity when Landau damping is lost as

$$I_{th} = \pm \frac{V}{2\pi h^2 Im\left(\frac{Z_e}{n}\right)} \left(\frac{1}{2}\sin\phi_l - \frac{\phi_l}{2} + 2\sin\frac{\phi_l}{2} - \phi_l \cos\frac{\phi_l}{2} \right) . \tag{61}$$

We consider the PS Booster parameters for the LHC beam. The bunch length needs to be expressed in radians. Using $f_{rf} = h \cdot f_{rev} = 600$ kHz we obtain

$$\phi_l = \phi_2 - \phi_1 = 2\pi f_{rf} t_b = 2\pi \cdot 600 \text{ kHz} \cdot 750 \text{ ns} = \frac{9\pi}{10} \text{ rad} . \tag{62}$$

Plugging these numbers into (61) with $h = 1$ yields, for the equivalent instability threshold

$$I_{th} = \pm \frac{8000V}{2\pi\left(\frac{376.73\Omega \cdot g}{2\beta\gamma^2}\right)} \left(\frac{1}{2}\sin\phi_l - \frac{\phi_l}{2} + 2\sin\frac{\phi_l}{2} - \phi_l \cos\frac{\phi_l}{2} \right) = 0.198343 \text{ A} . \tag{63}$$

The corresponding bunch population is given by,

$$N_{th} = \frac{I_{th} \cdot}{e f_{rev}} = 2.063 \cdot 10^{12} \text{ ppb} , \tag{64}$$

and divided into 12 LHC bunches,

$$N_{th}^{LHC} = 12 \frac{I_{th} \cdot}{e f_{rev}} = 1.71 \cdot 10^{11} \text{ , ppb} , \tag{65}$$

which is in nearly perfect agreement with the dipole-mode instability threshold obtained from the Sacherer formalism for the elliptic distribution with $n = 1/2$ (see Table 4).

C Frequency dependent space charge impedance

In principle, the space-charge impedance depends on the frequency in a more complicated manner. The following discussion shows that it is a good approximation to assume that Z/n is constant.

A fitting formula for the ratio of the Fourier-transformed potential and charge density was proposed by Bisognano. This ratio is exactly the expression for the geometric factor g, which has been assumed to be constant throughout this report. In a paper by G. Rumolo et al. [22] a modified Bisognano formula is given for the laboratory frame as

$$g = \frac{g_0}{1 + \frac{n^2}{\gamma^2}\frac{a^2}{4R^2}} \,, \tag{66}$$

where $g_0 = 1/2 + 2\ln(b/a)$ as before, R is the radius of the circumference and $n = \omega/\omega_{rev}$.

Hence, the space charge impedance times $1/n$ is frequency dependent. The effective impedance is given by

$$\left[\frac{Z_l(n)}{n}\right]^{eff}_{mm} = \frac{\sum\limits_{n=-\infty}^{n=+\infty} \frac{Z_l(\omega_{nm})}{n} h_{mm}(w_{nm})}{\sum\limits_{n=-\infty}^{n=+\infty} h_{mm}(w_{nm})} \,, \tag{67}$$

where, for a parabolic distribution with sinusoidal modes,

$$h_{mm}(\omega) = \frac{t_b^2}{2\pi^4}(|m|+1)^2)\frac{1 + (-1)^{|m|}\cos\omega t_b}{\left\{(\omega t_b/\pi)^2 - (|m|+1)^2\right\}^2} \tag{68}$$

and $\omega_{nm} = n\omega_{rev} + m\omega_s$ designates a displaced frequency.

The synchrotron tune for the PSB beam amounts to

$$Q_s = \frac{\omega_s}{\omega_{rev}} = \sqrt{\frac{|\eta| e h V_{rf}}{2\pi m_p \gamma \beta^2 c^2}} = \sqrt{\frac{0.840987 \cdot 8000eV}{2\pi 938 \cdot 10^6 eV \gamma \beta^2}} = 0.00335822 \,. \tag{69}$$

Thus, we have $\omega_n^l = (n + m \cdot Q_s)\omega_{rev} = 2\pi(6 \cdot 10^5 n + 2014.93m)$ Performing the numerical calculations now yields

$$\left[\frac{Z_l(n)}{n}\right]^{eff}_{00} = \left[\frac{Z_l(n)}{n}\right]^{eff}_{11} = 1758.01\ \Omega \,. \tag{70}$$

No difference of the effective impedances for the dipole or quadrupole modes from the constant space-charge impedance ($gZ_0/(2\beta\gamma^2)$ has been observed by using Bisognano's formula. Therefore, it is perfectly correct to assume that the space-charge impedance, divided by n, remains constant over the full frequency spectrum of beams in the PS Booster.